Available online at www.sciencedirect.com
ScienceDirect
Journal of Catalysis 245 (2007) 65–74
JOURNAL OF CATALYSIS
www.elsevier.com/locate/jcat

Comparative catalytic studies on the conversion of 1-butene and *n*-butane to isobutene over MCM-22 and ITQ-2 zeolites

Hye Ja Jung [a], Sang Soon Park [a], Chae-Ho Shin [b], Yong-Ki Park [c], Suk Bong Hong [a,*]

[a] *Division of Applied Chemistry and Biotechnology, Hanbat National University, Taejon 305-719, South Korea*
[b] *Department of Chemical Engineering, Chungbuk National University, Chungbuk 361-763, South Korea*
[c] *Division of Chemical Technology, Korea Research Institute of Chemical Technology, Taejon 305-606, South Korea*

Received 18 July 2006; revised 14 September 2006; accepted 16 September 2006

Available online 25 October 2006

Abstract

The catalytic properties of H-MCM-22 and Pt-MCM-22 for the skeletal isomerization of 1-butene and the dehydroisomerization of *n*-butane were compared with those obtained from their delaminated derivatives, H-ITQ-2 and Pt-ITQ-2. The overall results of our study strongly suggests that the desired 1-butene and *n*-butane conversions to isobutene in steady state occur mainly near the pore mouth inlets of the sinusoidal 10-ring channels retained in both of MCM-22 and ITQ-2 and inside this intralayer void space, respectively, which may be attributed to the unique geometric constraints imposed by the two-dimensionality of the pore system with a suitable degree of ellipticity of 10-ring channels. Whereas coke formation on the sinusoidal channels during the 1-butene skeletal isomerization can occur in such a way as to make most of the intrachannel Brønsted acid sites less available for nonselective dimerization-cracking reactions, it appears that the presence of H_2 in the *n*-butane dehydroisomerization stream would prevent extensive coke buildup, thereby allowing pore diffusion of reactants and products even in steady state.

Keywords: MCM-22 and ITQ-2; 1-Butene skeletal isomerization; *n*-Butane dehydroisomerization; Location of reactions

1. Introduction

MCM-22 (framework type MWW) is a high-silica zeolite first described by Rubin and Chu in 1990 [1]. This synthetic zeolite contains two independent pore systems, one defined by two-dimensional sinusoidal 10-ring (4.1 × 5.1 Å) channels and the other defined by large cylindrical supercages (7.1 Å in diameter and 18.2 Å in height) that are circumscribed by 12-ring channels but are accessible only through 10-ring (4.0 × 5.5 Å) windows [2]. Furthermore, most of the external surface of MCM-22 crystallites, which typically appear as very thin plates, is terminated by 12-ring cups or pockets (7.1 Å in diameter and 7.0 Å deep) that form as hemi-supercages, resulting from the truncation of the supercages described above.

Another interesting feature of MCM-22 is that it first crystallizes as a lamellar precursor that undergoes dehydroxylation on calcination between the layered sheets, to generate the so-called MWW structure. This has prompted Corma and co-workers to delaminate its lamellar precursor in a way similar to that applied to the exfoliation of clays, to provide access for bulky molecules to the catalytically active sites that would be otherwise excluded or sieved out by the 10-ring pores of the MWW structure [3–5]. Indeed, the resultant material, termed ITQ-2, has been shown to consist essentially of very thin (ca. 25 Å) sheets, the surface of which is formed by a hexagonal array of 12-ring pockets that penetrate into the sheet from both sides connected by a double 6-ring unit, but within which the large supercages no longer exist. But because the sinusoidal 10-ring channels are preserved inside the ITQ-2 sheet, this delaminated material retains zeolitic characteristics, together with a very high and structurally well-defined external surface area.

Over the past decade, due to the peculiar crystal structure of MCM-22, much attention has been directed to investigating its catalytic properties for numerous petrochemical reactions, such as isomerization, alkylation, and cracking [6–16]. Whereas the protonic acid sites located in the external 12-ring pockets have

* Corresponding author.
E-mail address: sbhong@hanbat.ac.kr (S.B. Hong).

0021-9517/$ – see front matter
doi:10.1016/j.jcat.2006.09.015

been shown to provide for the nest effect [17], making it possible to successfully commercialize the process for ethylbenzene production in Chiba, Japan [18], the shape selective properties of this zeolite have been considered generally intermediate between those of medium- and large-pore zeolites. In most of the hydrocarbon conversions studied thus far, however, the location of catalytically active sites responsible for the desired product formation over MCM-22 remains to be well defined, despite the lack of direct connection among its three pore systems that have different shapes and sizes and hence should show different shape selectivity effects. This also appears to be the case for the skeletal isomerization of 1-butene and the dehydroisomerization of *n*-butane in which H-MCM-22 and its Pt-loaded analog have been shown to be highly selective for isobutene formation [11,19]. Here we compare the catalytic properties of H-MCM-22 and Pt-MCM-22 zeolites for these two gas-phase reactions with those obtained from the practically supercage-free H-ITQ-2 and Pt-ITQ-2 materials, to elucidate the roles of the three pore systems of MWW-type zeolites in the production of isobutene, as well as in the formation of various byproducts via undesired consecutive reactions like dimerization followed by cracking into light hydrocarbons.

2. Experimental

2.1. Catalyst preparation

An MCM-22 zeolite with a Si/Al ratio of 16.8 was synthesized using hexamethyleneimine as an organic structure-directing agent (SDA) according to the procedures described in Ref. [20]. A portion of the crystallized product, frequently referred to as MCM-22(P), was calcined in air at 550 °C for 12 h, giving MCM-22, and then converted into the proton form by refluxing twice in 1.0 M NH_4NO_3 solutions (1.0 g solid per 100 ml solution) for 6 h, followed by calcination at 550 °C for 8 h. Another portion of MCM-22(P) was delaminated in accordance with the procedures developed by Corma et al. [3–5], to prepare the ITQ-2 sample. In a typical delamination experiment, 5.0 g of MCM-22(P) was first mixed with 28.2 g of hexadecyltrimethylammonium bromide (99%, Aldrich) and 60.1 g of tetrapropylammonium hydroxide (1.0 M aqueous solution, Aldrich) in 59.5 g of water and refluxed at 80 °C for 16 h. After the mixture was in an ultrasonic bath (100 W, 42 kHz) for 3 h, a few drops of 1.0 M HCl solution were added to adjust the pH to <2. The solid product was recovered by centrifugation, dried in air room temperature, and calcined at 550 °C for 6 h to remove the occluded organic species. The resulting ITQ-2 sample was converted into its proton form by refluxing twice in 1.0 M NH_4NO_3 solutions (1.0 g of solid per 100 ml of solution) for 6 h, followed by calcination at 550 °C for 8 h.

Pt loading onto the solid supports was done by ion exchange. Tetraamineplatinum(II) chloride monohydrate ($Pt(NH_3)_4Cl_2 \cdot H_2O$, 99%, Strem) was used as a Pt source. Typically, 40.9 mg of $Pt(NH_3)_4Cl_2 \cdot H_2O$ dissolved in 20 ml of water was added dropwise to a slurry of the ammonium form (2.0 g) of MCM-22 or ITQ-2 in 50 ml of water. After being stirred for 24 h, the powder was carefully filtered, washed repeatedly with water, and dried in air at room temperature. Subsequently, it was heated in air to 450 °C at a ramp rate of 0.5 °C min^{-1} and kept at the final temperature for 2 h.

2.2. Analytical methods

Powder X-ray diffraction (XRD) patterns were collected on a Siemens D-5000 diffractometer with CuK_α radiation. Elemental analysis for Al, Si, and Pt was carried out at the Analytical Laboratory of Korea Institute of Science and Technology, using a Jarrell–Ash Polyscan 61E inductively coupled plasma (ICP) spectrometer in combination with a Perkin–Elmer 5000 atomic absorption spectrophotometer. Thermogravimetric analysis (TGA) was performed in air on a TA Instruments SDT 2960 thermal analyzer, where the weight loss related to the combustion of coke deposits formed during the 1-butene skeletal isomerization or the *n*-butane dehydroisomerization was further confirmed by differential thermal analysis (DTA) using the same analyzer. The N_2 sorption experiments were performed on a Micromeritics ASAP 2010 analyzer. Temperature-programmed desorption (TPD) of NH_3 was recorded on a fixed-bed, flow-type apparatus attached to a Balzers TCP 015 quadruple mass spectrometer. About 0.1 g of sample was first activated in flowing He at 500 °C for 1 h, then pure NH_3 (50 cm^3 min^{-1}) was passed over the sample at 150 °C for 0.5 h. The treated sample was subsequently purged with He at the same temperature for 1 h to remove the physisorbed NH_3. Finally, the TPD profiles were obtained in flowing He (100 cm^3 min^{-1}) from 150 to 650 °C at a heating rate of 10 °C min^{-1}.

The IR spectra in the structural region were measured on a Nicolet Magna 550 FT-IR spectrometer using the KBr pellet technique. The relative ratios of tetrahedral and octahedral Al species in H-MCM-22 and H-ITQ-2 materials prepared here were determined by ^{27}Al MAS NMR spectroscopy. The experiments were performed on a Bruker Avance 500 spectrometer at a spinning rate of 10.0 kHz. The operating ^{27}Al frequency was 130.325 MHz, and the spectra were obtained with an acquisition of ca. 1000 pulse transients, which were repeated with a $\pi/8$ rad pulse length of 1.2 μs and a recycle delay of 1 s. The ^{27}Al chemical shifts are referenced to an $Al(H_2O)_6^{3+}$ solution. Transmission electron microscopy (TEM) was applied to study the size and location of Pt clusters or particles. The measurements were performed on a JEOL JEM-2010 electron microscope operating at an acceleration voltage of 200 kV. The samples were grounded and deposited from a suspension in methanol onto a holey carbon grid.

2.3. Catalysis

All of the catalytic experiments were carried out under atmospheric pressure in a continuous-flow apparatus with a fixed-bed microreactor. In the skeletal isomerization of 1-butene, the catalyst was activated under flowing He (50 cm^3 min^{-1}) at 500 °C for 1 h and kept at 350 or 500 °C to establish a standard operating procedure, allowing time for the product distribution to stabilize. Then, a reactant stream of 10% 1-butene in He as

a balancing gas was fed into a quartz reactor containing 0.10–0.22 g of zeolite catalyst at the same temperature. The total gas flow at the reactor inlet was kept constant at 50 $cm^3\,min^{-1}$. In the dehydroisomerization of *n*-butane, 0.1 g of the catalyst was reduced in situ with flowing 20% H_2 in He (50 $cm^3\,min^{-1}$) at 500 °C for 2 h. The reaction was started by feeding a reactant stream of 10% *n*-butane and 20% H_2 in He as a balancing gas, and the total gas flow was fixed to 50 $cm^3\,min^{-1}$. The reaction products from both reactions were analyzed on-line in a Chrompack CP 9001 gas chromatograph equipped with an Al_2O_3/KCl Plot capillary column (0.53 mm × 50 m) and a flame ionization detector, with the first analysis carried out after 3 min on stream. Conversion to, selectivity to, and yield in each product were calculated as described previously [19,21].

3. Results and discussion

Fig. 1 shows the powder XRD patterns of MCM-22(P), H-MCM-22, swollen MCM-22(P), and H-ITQ-2 prepared in this study. The XRD pattern of each material agrees well with that of the corresponding material in Refs. [3,4]. The lack of (001) and (002) reflections at $2\theta = 3°–7°$ in the pattern of H-ITQ-2 indicates a significant reduction of long-range order along the *c* axis on exfoliation of MCM-22(P). Fig. 2 compares the IR spectra in the structural region of H-MCM-22 and H-ITQ-2. As reported previously [3,4], a band at around 960 cm^{-1}, which corresponds to SiOH groups and is hardly visible in the spectrum of H-MCM-22, is clearly resolved in that of H-ITQ-2. This reveals the presence of a much larger amount of terminal SiOH groups in the latter zeolite, due to its delaminated nature. The successful formation of ITQ-2 can be further supported by the N_2 BET surface area data in Table 1. The fact that the external (or mesoporous) surface area of H-ITQ-2 is approximately six times larger than that of H-CM-22 suggests that ITQ-2 prepared here is mostly formed by single layers. The powder XRD patterns (not shown) of Pt-MCM-22 and Pt-ITQ-2 after reduction were found to be essentially the same as those of their proton form, respectively, except the minor change in relative X-ray peak intensities. Elemental analysis indicates that the Pt content (0.62 wt%) of Pt-MCM-22 is slightly higher than that (0.51 wt%) of Pt-ITQ-2, although the identical Pt^{2+} ion exchange conditions were applied to the preparation of both materials. This can be rationalized by considering that the bulk Si/Al ratio (16.8) of H-MCM-22 is slightly lower than that (19.2) of H-ITQ-2 (Table 1). As described above, the preparation procedure of ITQ-2 includes the use of some concentrated HCl to keep the pH of the sonicated mixture as low as 2 before separation. Therefore, it is not very difficult to predict that a minor part of Al atoms has been extracted from the MCM-22(P) framework during the delamination process, explaining why H-ITQ-2 has a slightly lower Al content than H-MCM-22.

Fig. 3 shows the ^{27}Al MAS NMR spectra of MCM-22(P), H-MCM-22, and H-ITQ-2. The spectra of Pt-MCM-22 and Pt-ITQ-2 are also given in Fig. 3. MCM-22(P) exhibits two tetrahedral ^{27}Al resonances around 50 and 56 ppm. In con-

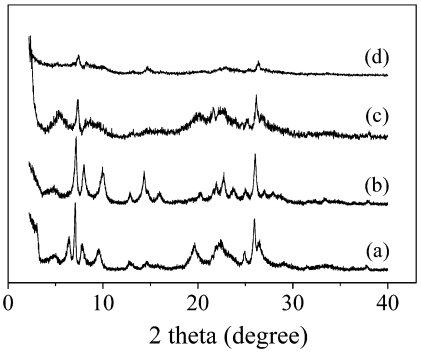

Fig. 1. Powder XRD patterns of (a) MCM-22(P), (b) H-MCM-22, (c) swollen MCM-22(P), and (d) H-ITQ-2 prepared in this study.

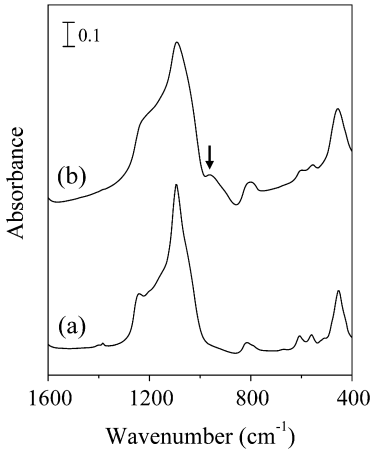

Fig. 2. IR spectra in the structural region of (a) H-MCM-22 and (b) H-ITQ-2. The band characteristic of SiOH groups is marked with an arrow.

Table 1
Characterization data for zeolite catalysts prepared in this study

Catalyst	Si/Al ratio[a]	Pt wt%[a]	BET surface area[b] ($m^2\,g^{-1}$)			$Al_{Oh}/(Al_{Oh}+Al_{Td})$[e](%)
			Total	External[c]	Microporous[d]	
H-MCM-22	16.8	–	462	105	357	15
Pt-MCM-22	17.0	0.62	447	98	349	20
H-ITQ-2	19.2	–	729	669	59	12
Pt-ITQ-2	19.9	0.51	694	648	46	13

[a] Determined by elemental analysis.
[b] Calculated from N_2 adsorption data.
[c] Calculated using the *t*-plot method.
[d] Difference between the total and external surface areas.
[e] Calculated from ^{27}Al MAS NMR data.

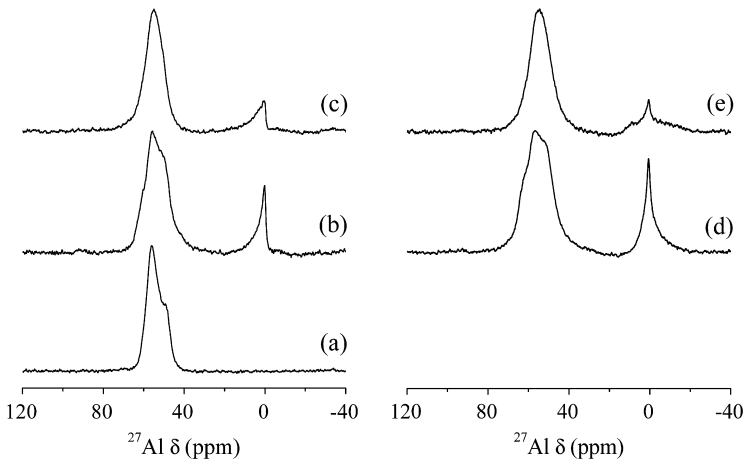

Fig. 3. ^{27}Al MAS NMR spectra of (a) MCM-22(P), (b) H-MCM-22, (c) H-ITQ-2, (d) Pt-MCM-22, and (e) Pt-ITQ-2.

trast, H-MCM-22 gives an additional shoulder around 61 ppm, as well as a signal around 0 ppm attributable to octahedral Al. These spectral data are in good agreement with those reported previously [22–24]. Like H-MCM-22, H-ITQ-2 shows one octahedral ^{27}Al resonance around 0 ppm. As shown in Fig. 3, however, the tetrahedral resonance around 50 ppm that has been tentatively assigned to Al atoms in sites T_6 and T_7 of the hexagonal model of the MCM-22 structure [22], where eight crystallographically distinct tetrahedral sites (T sites) exist [2], is hardly visible in the ^{27}Al MAS NMR spectrum of H-ITQ-2, despite the fact that both materials were prepared using the same staring material, that is, MCM-22(P). Thus, if we assume that the available T sites in the proposed structure of ITQ-2 are exactly the same as those in the hexagonal MWW structure, then the extent of dealumination from the ITQ-2 framework during preparation of this laminated material should be considerably higher on the Al atoms in sites T_6 and T_7 than those in the other six T sites, unlike the case of the three-dimensional MCM-22 zeolite. This is somewhat unexpected, because the average T_6-O-T and T_7-O-T angles (161.5° and 158.5°) derived from the Rietveld refinement [2] of the synchrotron powder XRD data for a calcined borosilicate MCM-22 are higher than any of the other six average T_n-O-T angles, where $n = 1$–5 and 8 [22], and hence because sites T_6 and T_7 are relatively less strained. Furthermore, sites T_6 and T_7 are not on the surface of the MWW double layer consisting of two sheets of small $\{4^3 5^6 6^3 [4^3]\}$ cages. Thus, they can be expected to be sterically less accessible to HCl, added before separation of the sonicated mixture, than the other sites, such as T_1 or T_2 exposed to the ITQ-2 sheet exterior, due to their location in the wall of the external 12-ring pockets after delamination. Although elucidating the origin of the nonrandom nature of dealumination in ITQ-2 is beyond the scope of this paper, the ^{27}Al MAS NMR spectra in Fig. 3 clearly show that the actual distribution of Al atoms over the available T sites in H-ITQ-2 differs from that in H-MCM-22. Assuming that all Al atoms in these two materials are detected in their ^{27}Al MAS NMR spectra and no intensity loss is caused by the presence of NMR "invisible" extra-framework Al species [25], curve deconvolution indicates that H-MCM-22 and H-ITQ-2 have comparable fractions of octahedral Al

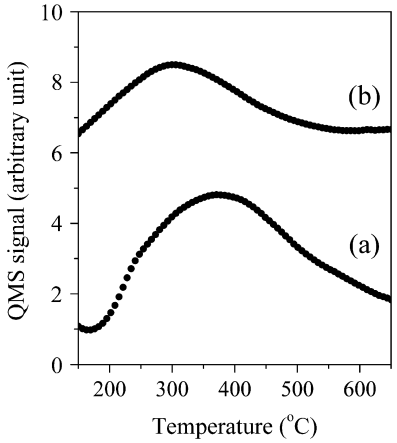

Fig. 4. NH_3 TPD profiles from (a) H-MCM-22 and (b) H-ITQ-2.

(Table 1). We also note that the ^{27}Al MAS NMR spectra of Pt-MCM-22 and Pt-ITQ-2 in the tetrahedral framework region are characterized by line shapes that are essentially identical to those seen for H-MCM-22 and H-ITQ-2, respectively. It thus appears that the Al distribution patterns in MCM-22 and ITQ-2 remain almost unchanged during the Pt loading step, that is, ion exchange followed by calcination. Unlike Pt-ITQ-2, however, Pt-MCM-22 gave a higher fraction of octahedral Al compared with its proton form, which is consistent with the trend reported by Lercher et al. [19]. This suggests that the extent of dealumination caused by incorporation of Pt is higher for Pt-MCM-22 than for Pt-ITQ-2, although the precise reason for this remains unclear.

Fig. 4 shows the NH_3 TPD profiles obtained from H-MCM-22 and H-ITQ-2 prepared here. The TPD profile of H-MCM-22 is characterized by one broad and asymmetric desorption peak with maxima in the temperature region 370–380 °C, assignable to NH_3 desorption from strong acid sites. As seen in Fig. 4, however, the desorption peak from H-ITQ-2 is located at a lower temperature (maximum around 310 °C). Here we cannot exclude the effects of the difficulty of trapping desorbed NH_3 molecules in the external pockets on the TPD profile of H-ITQ-2, due to its delaminated nature. As expected from the bulk Si/Al ratios given in Table 1, in addition, the total area

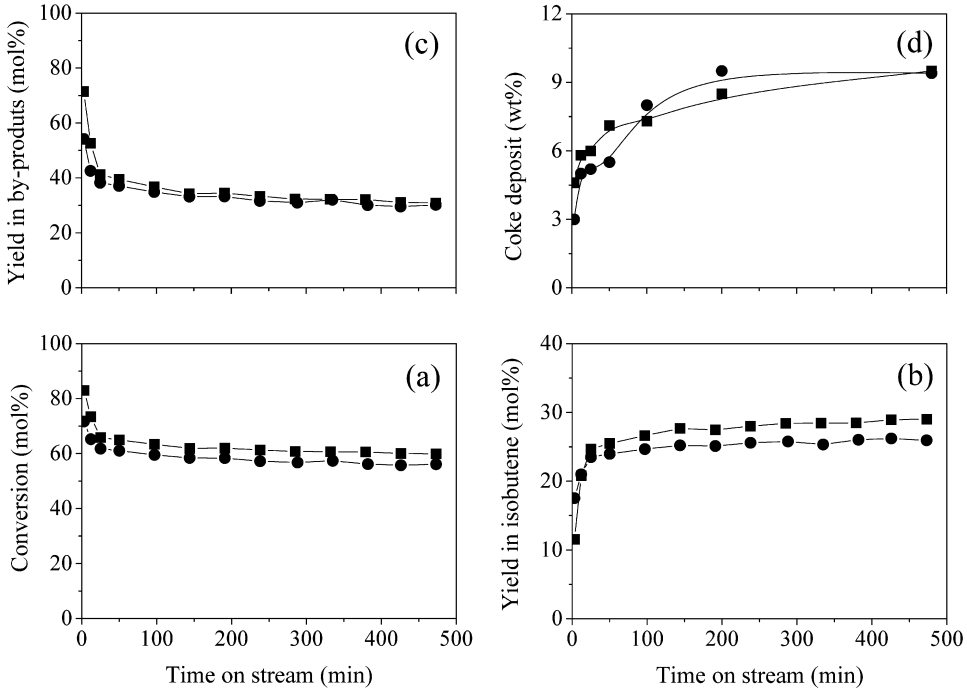

Fig. 5. (a) 1-Butene conversion, yields in (b) isobutene and (c) major by-products (i.e., propene and pentenes), and (d) coke formation as a function of time on stream in skeletal isomerization of 1-butene over H-MCM-22 (■) and H-ITQ-2 (●) at 350 °C and 10% 1-butene in the feed.

of NH_3 desorption (i.e., the density of acid sites) was lower for H-ITQ-2 and for H-MCM-22. It is well established that the acidity and pore structure of zeolites are the two important factors determining their activity and selectivity during the skeletal isomerization of 1-butene [26,27], which is also the case of various zeolite-supported Pt catalysts for the dehydroisomerization of *n*-butane [28]. Because the NH_3 TPD results in Fig. 4 reveal that differences in the number and strength of acid sites between H-MCM-22 and H-ITQ-2 prepared here are not so large, comparison not only of the isomerization activities of these two zeolites, but also of the dehydroisomerization activities of their Pt-loaded analogs with similar metal loading levels will allow us to discriminate among the roles of three different pore systems of MWW-type zeolites in the desired conversion of 1-butene and *n*-butane to isobutene.

Fig. 5 shows 1-butene conversion and yields in isobutene and major byproducts (i.e., propene and pentenes) as a function of time on stream (TOS) in the skeletal isomerization of 1-butene over H-MCM-22 and H-ITQ-2 measured at 350 °C and 10% 1-butene in the feed. To make the comparison of the product distributions in 1-butene skeletal isomerization over these two catalysts as meaningful as possible, we attempted to maintain their 1-butene conversions similar to one another during the period of TOS studied here, by changing the amount of catalyst in the reactor. The TOS effects on coke formation over H-MCM-22 and H-ITQ-2 are also given in Fig. 5. Although it was difficult to achieve similar conversions for the first 10 min on stream, probably due to the difference in their intrinsic isomerization activities, both H-MCM-22 and H-ITQ-2 exhibited a low isobutene yield at the beginning of the reaction while producing large amounts of byproducts (mainly propene and pentenes). This indicates that the initial isobutene formation is dominated by nonselective bimolecular reactions, that is, dimerization and subsequent cracking. As described above, the large interconnecting supercages with smaller connecting 10-ring (4.0 × 5.5 Å) windows, typical for MCM-22 but no longer for ITQ-2, are circumscribed by 12-rings so that they do not have shape selectivity to effectively suppress nonselective side reactions, which must also be the case for external 12-ring pockets existing in a much greater quantity on ITQ-2. In addition, the free diameter (5.8 Å) at the intersection of the two sinusoidal 10-ring channels retained in both of MCM-22 and ITQ-2 is fairly larger than that (5.2 Å) at the intersection of the 10-ring (4.2 × 5.4 Å) and 8-ring (3.5 × 4.8 Å) channels in ferrierite (FER), which is the best catalyst among the zeolites tested thus far for the skeletal isomerization of 1-butene but is characterized by low initial isobutene selectivity [26,27]. This indicates that the sinusoidal channel intersection in MWW-type zeolites is also large enough to accommodate two *n*-butenes and undergo nonselective dimerization-cracking reactions, like that in FER, explaining the low isobutene yield observed for fresh H-MCM-22 and H-ITQ-2.

The most interesting result obtained from Fig. 5 is that both catalysts show a rapid increase in isobutene yield at early TOS, together with a simultaneous decrease in formation of byproducts, and then a stable product distribution over the rest of the TOS period studied. A quite similar trend was also observed for the catalytic experiments carried out at the reaction temperature (500 °C) of *n*-butane dehydroisomerization. This strongly suggests that after some TOS, the prevailing mechanism for isobutene formation over these two zeolites becomes altered, which cannot be understood without considering the positive effect of coke formation on their isomerization activities [26, 27,29–33]. Due to the reasons described above, one cannot

claim that the pore dimensions of supercages and external pockets are properly altered by coke deposition to significantly enhance shape selectivity with TOS, although poisoning by coke of the nonselective acid sites in these large cavities could lead to some enhancement of isobutene selectivity. Nevertheless, Fig. 5 shows that coke formation on H-MCM-22 and H-ITQ-2 coincides with their selective behavior in 1-butene skeletal isomerization and that the difference in the amounts (∼9 wt%) of coke deposited on these two catalysts after 480 min on stream of isomerization at 350 °C is essentially zero. It should also be noted that this coke level is quite similar not only to the steady-state amount (8–9 wt%) of coke on H-FER during the reaction at the same temperature [27], but also to that (∼9 wt%) on the corresponding catalysts at 500 °C, which led us to turn our attention to the role of coke deposited within their sinusoidal 10-ring (4.1 × 5.1 Å) channels.

Undoubtedly, the pore size of zeolites and related microporous materials is the most important feature with regard to coke formation and consequently for isobutene selectivity and stability as well, because all microporous materials reported as selective isomerization catalysts have 10-ring channels. However, not all medium-pore materials are selective for this reaction. In particular, the high selectivity together with fairly good stability is observed only over the aged H-FER catalyst with coke deposits present. Although the prevailing mechanism in the selective formation of isobutene over aged H-FER is still subject to vigorous debate [26,27,29–33], there is a general consensus that after some TOS, the H-FER pores are largely filled by coke, with catalysis occurring primarily near the 10-ring pore mouth inlets. We believe that this may also be the case for aged H-MCM-22 and H-ITQ-2. Our recent studies on the isomerization activities of the proton form of a number of medium-pore zeolites, including clinoptilolite (HEU), FER, ZSM-22 (TON), SUZ-4, ZSM-57 (MFS), ZSM-5 (MFI), and TNU-10 (STI), with different structures have shown that in general, the more elliptical 10-ring channels the zeolite has, the lower the 1-butene conversion but the higher initial isobutene selectivity the zeolite shows [32,34]. Such a trend is also observed when the catalytic data are obtained after 8 h on stream, and hence after coke formation at certain levels on this series of zeolites. In contrast, no general relationship between the isomerization activity of each zeolite and its 10-ring pore area, dimensionality, or amount of coke deposited was found. These results have led us to focus on the pore shape of the 10-ring channels in medium-pore zeolites as a more crucial parameter substantially influencing the chemisorption of 1-butene molecules near the pore mouths and thus the isomerization activity. When the ellipticity (ε), defined by $\{(b^2 - a^2)/b^2\}^{0.5}$, where a and b are the shortest and longest pore diameters, respectively, is taken as a quantitative measure of differences in the 10-ring pore shape, the ε value of the sinusoidal 10-ring channels in H-MCM-22 or H-ITQ-2 was calculated to be 0.595. This value is essentially the same as that (0.591) calculated for H-ZSM-22, which is also among the most active zeolite catalysts for the isomerization reaction [26,27], and is slightly lower than that (0.629) of the analogous channels in H-FER [32]. Therefore, we believe that the selective behavior of aged H-MCM-22 and H-ITQ-2 for isobutene formation may originate mainly from the unique pore structure of their intralayer channel system, within which coke formation occurs in such a way as to effectively suppress nonselective dimerization-cracking reactions, but for which most of the 10-ring pore mouth inlets with a suitable degree of ellipticity are still accessible for 1-butene molecules even after the buildup of a considerable amount of coke inside the sinusoidal channels, as well as inside the large supercages or on the external pockets. If this were the case, then the catalytic results in Fig. 5 could then provide another piece of experimental evidence in support of our recent claim that the positive effect of coke deposits on the isobutene selectivity is not unique only with H-FER among the already known medium-pore zeolites [32].

Fig. 6 shows n-butane conversion and yields in isobutene and various major byproducts as a function of TOS in the dehydroisomerization of n-butane over 0.6% Pt-MCM-22 and 0.5% Pt-ITQ-2 measured at 500 °C, 7.8 h^{-1} WHSV, and 10% n-butane and 20% H_2 in the feed. Pt-MCM-22 exhibits a significantly higher initial n-butane conversion (87% vs 51%) than Pt-ITQ-2, whereas the opposite is observed for the yield in isobutene (3% vs 7%). As a result, their initial byproduct patterns differ significantly. For the former, methane is the most dominant byproduct; for the latter, however, the main byproducts are linear butenes and propane and, to a lesser extent, isobutene, methane, and ethane. We also note that both Pt-MCM-22 and Pt-ITQ-2 hardly show any production of pentene, indicating a negligible contribution of dimerization of butenes (formed by dehydrogenation over Pt) followed by cracking to overall byproduct formation at the beginning of the reaction. This is not unexpected, because 1-butene dimerization is not thermodynamically favored at higher reaction temperatures [11]. In fact, we found that the initial molar ratios of propene to pentenes in the skeletal isomerization of 1-butene over H-MCM-22 and H-ITQ-2 measured at 500 °C (i.e., the reaction temperature of n-butane dehydroisomerization) are one order of magnitude larger than the values over the corresponding catalysts at 350 °C. Then three types of side reactions can be proposed for the initial byproduct formation in dehydroisomerization over Pt-MCM-22 and Pt-ITQ-2: protolytic cracking of n-butane, hydrogenolysis of n-butane, and cracking of butenes followed by hydrogenation [35]. Given that Pt-MCM-22 produces a much larger amount of methane compared with the sum of propane and propene, hydrogenolysis over the metal in this catalyst appears to be the major source of methane. Moreover, the fact that the yields in methane and ethane decease rapidly with TOS suggests that they are formed by the same reaction (i.e., hydrogenolysis). In contrast, the high initial yield in propane observed for Pt-ITQ-2 implies that hydrogenation of propene, a butene-cracking product, over Pt in this layered zeolite is the main side reaction. We speculate that such a notable difference in the initial hydrogenolysis activities of these two catalysts may originate mainly from the difference in their metal dispersions (see below). But on the other hand, as shown in Fig. 6, Pt-MCM-22 shows a rapid decrease in n-butane conversion with increasing TOS, along with a significant increase in isobutene and n-butene yields, in good agreement with the

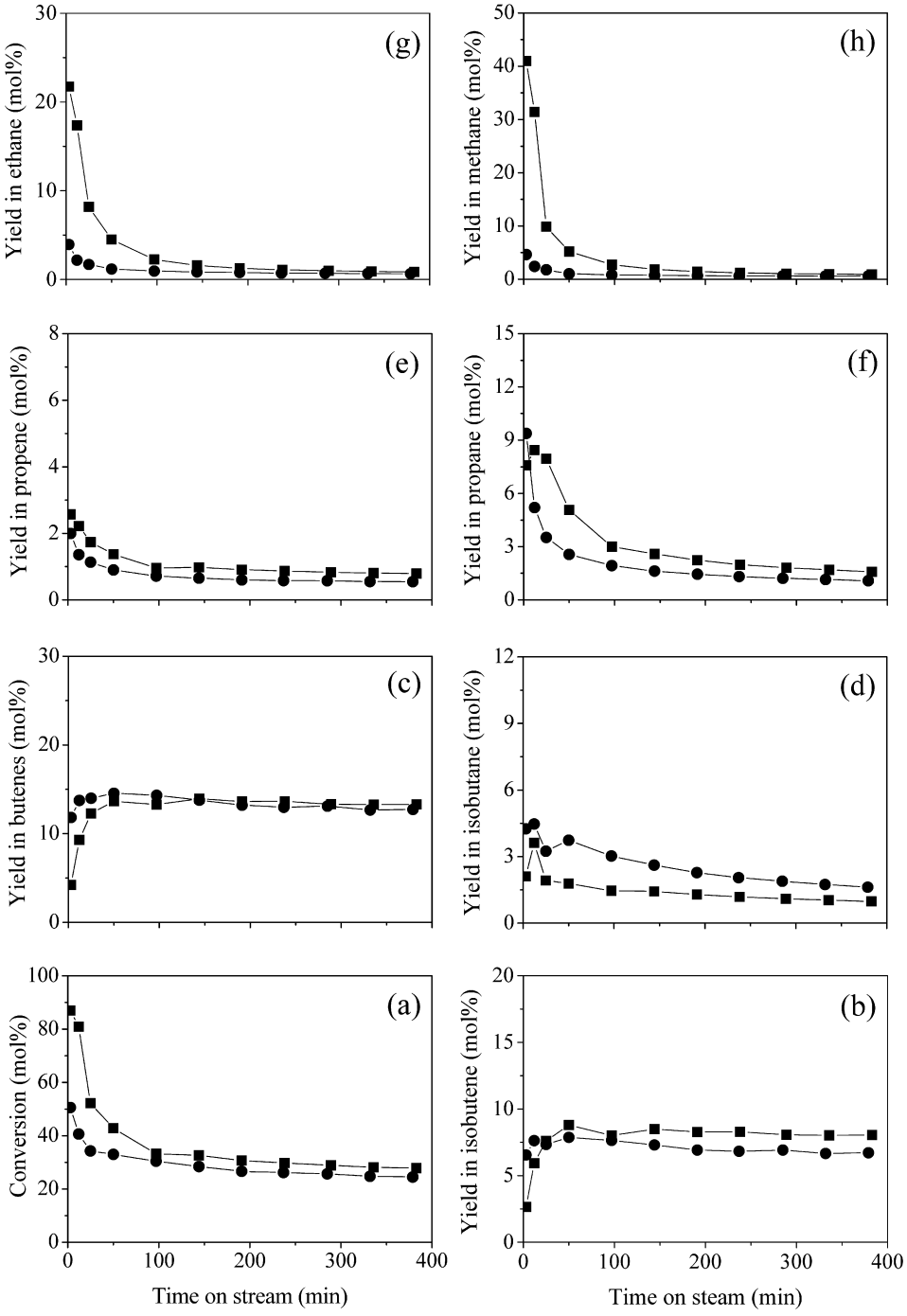

Fig. 6. (a) *n*-Butane conversion and yields in (b) isobutene, (c) *n*-butenes, (d) isobutane, (e) propene, (f) propane, (g) ethane, and (h) methane as a function of time on stream in dehydroisomerization of *n*-butane over 0.6% Pt-MCM-22 (■) and 0.5% Pt-ITQ-2 (●) at 500 °C, 7.8 h^{-1} WHSV, and 10% *n*-butane and 20% H_2 in the feed.

findings of Lercher et al. [19]. A similar TOS behavior can also be observed for Pt-ITQ-2. However, note that this catalyst gives much lower decreases in *n*-butane conversion and in methane and ethane yields at early TOS than Pt-MCM-22. Consequently, not only the *n*-butane conversions of these two catalysts, but also their isobutene yields become almost identical after 100 min on stream.

Fig. 7 shows the steady-state selectivities of Pt-MCM-22 and Pt-ITQ-2 to isobutene and *n*-butenes and their molar fractions of isobutene to all butenes (i.e., the $i\text{-}C_4^= / \sum C_4^=$ ratio) recorded as a function of *n*-butane conversion at 500 °C and 100 min on stream. It can be seen that the isobutene selectivities of these two catalysts decreases with increasing *n*-butane conversion but are comparable over the conversion range studied here. A quite similar result was obtained from their selectivities to *n*-butenes. When the $i\text{-}C_4^= / \sum C_4^=$ ratio is taken as a measure of the isomerization activity, Pt-MCM-22 and Pt-ITQ-2 exhibit essentially identical activities (∼37%), slightly lower than the thermodynamic limit of 43%, which are invariable with *n*-butane conversion. This clearly shows that after stabilization, Pt-MCM-22

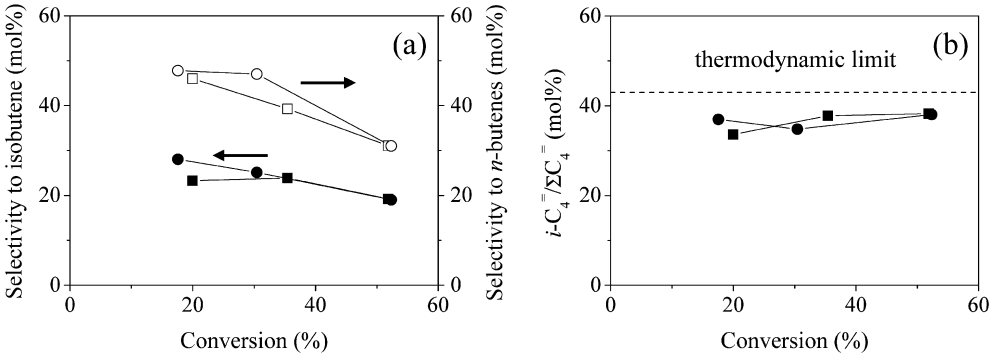

Fig. 7. (a) Selectivities to isobutene (closed symbols) and *n*-butenes (open symbols) and (b) $i\text{-}C_4^= / \sum C_4^=$ ratio as a function of *n*-butane conversion in dehydroisomerization of *n*-butane over Pt-MCM-22 (squares) and Pt-ITQ-2 (circles) measured at 500 °C, 100 min on stream, and 10% *n*-butane and 20% H_2 in the feed.

and Pt-ITQ-2 behave in a comparable manner. Fig. 8 compares their stabilities during *n*-butane dehydroisomerization under the conditions described in Fig. 6. The initial dehydrogenation activity (i.e., the yield in $\sum C_4^=$) of Pt-MCM-22 was significantly lower than that of Pt-ITQ-2, possibly related to its higher initial hydrogenolysis activity (see above). As shown in Fig. 8, however, the dehydrogenation activity of the former increases rapidly for the first 50 min on stream. As a result, Pt-MCM-22 and Pt-ITQ-2 have nearly the same dehydrogenation activity over the rest period of TOS studied, although the latter shows a slight deactivation. Hydrogenolysis is a structure-sensitive reaction that competes with structure-insensitive dehydrogenation over the metal [36]. Therefore, the rapid increase in dehydrogenation activity with increasing TOS observed for Pt-MCM-22 can be rationalized by suggesting that some of its Pt particles are small enough to easily sinter under the reaction conditions used here, leading to decreased formation of hydrogenolysis products. Whereas the isomerization activity of Pt-MCM-22 is larger by a narrow margin than that of Pt-ITQ-2 from the beginning of the reaction, almost no TOS dependence on isomerization activity is observed. Fig. 8 also shows the influence of TOS on coke formation over Pt-MCM-22 and Pt-ITQ-2. We note that the amount of coke deposited after 380 min on stream of dehydroisomerization at 500 °C, as well as the coke formation pattern, is nearly the same for these two catalysts.

Fig. 9 shows the TEM pictures of Pt-MCM-22 and Pt-ITQ-2 before and after their use in *n*-butane dehydroisomerization under the conditions described above. In general, Pt particles cannot be observed in fresh Pt-MCM-22, suggesting that they are well dispersed over the MCM-22 crystallites. The average Pt particle size of used Pt-MCM-22 must be close to that of the fresh catalyst, because no large Pt particles are observed even after exposure to reaction conditions. This indicates that Pt particles in MCM-22 do not migrate to the surface of the catalysts at reaction conditions (500 °C) in a period of about 6 h. Because there is a trend of rapidly increasing dehydrogenation activity at early TOS (Fig. 8), however, we cannot rule out the possibility that the sintering of very small Pt particles (<10 Å) that remain within the micropores of MCM-22, especially within its supercages, occurs during the reaction. It has been repeatedly shown that the particle size distribution of highly dispersed Pt particles in zeolites determined by TEM is very sensitive to experimental conditions, because the zeolite framework is easily damaged when the incident beam is sufficiently strong (200 kV) [37,38]. For fresh Pt-ITQ-2, in contrast, Pt particles with diameters of 50–100 Å were found. This suggests that Pt is distributed

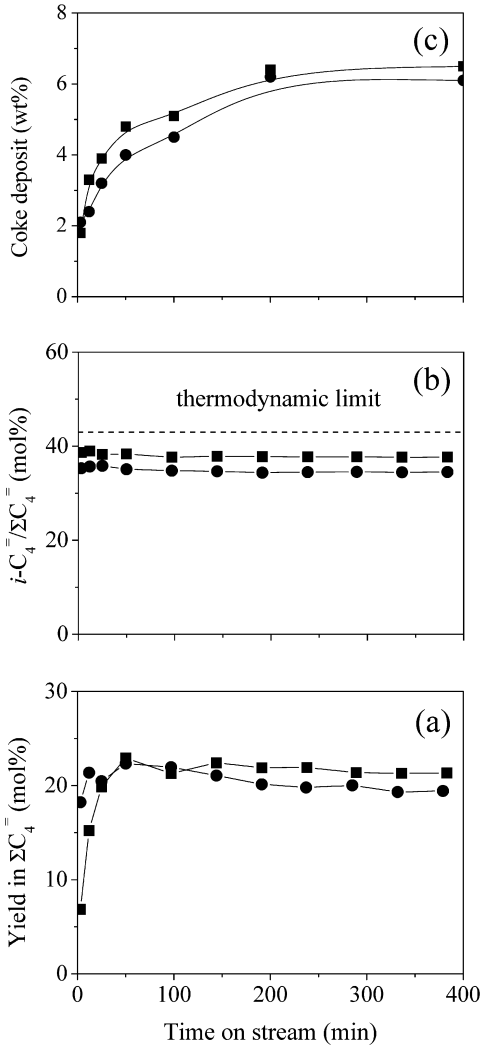

Fig. 8. (a) Dehydrogenation and (b) isomerization stabilities and (c) coke formation as a function of time on stream in dehydroisomerization of *n*-butane over Pt-MCM-22 (■) and Pt-ITQ-2 (●). The reaction conditions are the same as those given in Fig. 6.

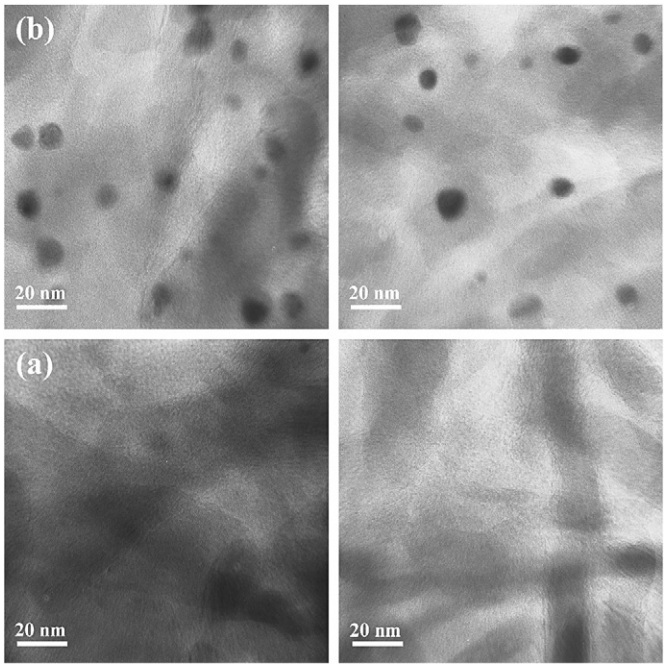

Fig. 9. Transmission electron micrographs of (a) Pt-MCM-22 and (b) Pt-ITQ-2 before (left) and after (right) their use in dehydroisomerization of *n*-butane at 500 °C, 7.8 h^{-1} WHSV, and 10% *n*-butane and 20% H_2 in the feed for 380 min.

randomly throughout the intracrystalline pores as well as on the external surface of the delaminated crystallites. Because there are no noticeable differences in the average particle size of fresh and used Pt-ITQ-2 catalysts, like the case of Pt-MCM-22, it appears that the reduction of Pt-ITQ-2 at 500 °C may result in the migration and agglomeration of $Pt(NH_3)_4^{2+}$ ions exchanged onto its external 12-ring pockets, where there is no beneficial effect of the micropores.

With bifunctional metal-loaded zeolite catalysts for the dehydroisomerization of *n*-butane, in general, the dehydrogenation over the metal is the first step, followed by isomerization over the Brønsted acid sites in zeolite supports [28,35]. The TEM results in Fig. 9 reveal that most, if not all, of the Pt particles in the used MCM-22 catalyst are still intrazeolitic. Thus, the main location of selective dehydroisomerization sites cannot be on its external 12-ring pockets. We believe that this is also the case of Pt-ITQ-2 containing much larger Pt particles (50–100 Å) compared with Pt-MCM-22, because the steady-state catalytic behavior is essentially the same for these two catalysts (Figs. 6–8). In fact, it has been shown that dehydrogenation activity of Pt-loaded zeolite catalysts is not directly related to the metal dispersion [28]. Due to the inherently shape-selective nature of zeolites, on the other hand, coke formation on these microporous materials is also a shape-selective process that depends highly on pore architecture [39,40]. Because the rates of coke formation over zeolites containing large cavities with windows of smaller size are normally higher than those over medium-pore zeolites with 10-ring pores of uniform dimension, leading to rapid deactivation, it is not difficult to infer that the selective dehydroisomerization sites, especially in steady state, cannot be located within the large supercages. Therefore, it is most likely that the intralayer 10-ring pore system may be ultimately responsible for the high dehydroisomerization activity observed for Pt-MCM-22 and Pt-ITQ-2 after some TOS. We should note here that the steady-state amounts (6 wt%) of coke formed on Pt-MCM-22 and Pt-ITQ-2 during the dehydroisomerization at 500 °C are fairly smaller than those (9 wt%) of coke on H-MCM-22 and H-ITQ-2 during 1-butene isomerization at the same temperature, due mainly to the presence of H_2 in the former reaction stream. Given the two-dimensionality of the sinusoidal pore system, this suggests that diffusion of the reactants and products imposed by coke formation would not be so severe, as in the case of Pt-ZSM-5 with two intersecting 10-ring channels, which is among the most active catalysts for *n*-butane dehydroisomerization [28].

4. Conclusion

Skeletal isomerization of 1-butene and dehydroisomerization of *n*-butane at atmospheric pressure have been investigated over the proton form of MCM-22 and ITQ-2 and their Pt-loaded analogs. The two-dimensional sinusoidal 10-ring channels of these zeolites were found to play a much more crucial role in the selective production of isobutene than the large supercages or the 12-ring external pockets. The rate of coke formation appears to be much faster on the protonic sites of the latter two pore systems, probably due to the greater coke-forming tendency, leading to suppression of undesired consecutive reactions such as dimerization cracking at early TOS in these larger cavities. The overall results of our study lead us to conclude that isobutene formation over stabilized H-MCM-22 and H-ITQ-2 occurs mainly near the pore mouth inlets of sinusoidal 10-ring channels, whereas the selective sites for *n*-butane dehydroisomerization over Pt-MCM-22 and Pt-ITQ-2 in steady state are located inside this intralayer pore system.

Acknowledgments

Funding for this work was provided by the Korea Research Foundation (grant 2004-D00172 to S.B.H.). The authors thank Professor G. Seo, Chonnam National University, for the NH_3 TPD measurements.

References

[1] M.K. Rubin, P. Chu, U.S. patent 4,954,325, 1990.
[2] M.E. Leonowicz, J.A. Lawton, S.L. Lawton, M.K. Rubin, Science 264 (1994) 1910.
[3] A. Corma, V. Fornes, S.B. Pergher, Th.L.M. Maesen, J.G. Buglass, Nature 396 (1998) 353.
[4] A. Corma, V. Fornes, J. Martinez-Triguero, S.B. Pergher, J. Catal. 186 (1999) 57.
[5] A. Corma, V. Fornes, J.M. Guil, S.B. Pergher, Th.L.M. Maesen, J.G. Buglass, Micropor. Mesopor. Mater. 38 (2000) 301.
[6] A. Corma, C. Corell, A. Martinez, J. Perez-Pariente, Stud. Surf. Sci. Catal. 84 (1994) 859.
[7] A. Corma, C. Corell, F. Llopis, A. Martinez, J. Perez-Pariente, Appl. Catal. A 115 (1994) 121.
[8] A. Corma, A. Martinez, C. Martinez, Catal. Lett. 28 (1994) 87.
[9] W. Souverijins, W. Verrelst, G. Vanbustsele, J.A. Martens, P.A. Jacobs, J. Chem. Soc. Chem. Commun. (1994) 1671.

[10] A. Corma, V. Gonzalez-Alfaro, A.V. Orchilles, Appl. Catal. A 129 (1995) 203.
[11] M.A. Asensi, A. Corma, A. Martinez, J. Catal. 158 (1996) 561.
[12] A. Corma, J. Martinez-Triguero, J. Catal. 165 (1997) 102.
[13] P. Meriaudeau, Vu.A. Tuan, Vu.T. Nghiem, F. Lefevbre, Vu.T. Ha, J. Catal. 185 (1999) 378.
[14] I. Rodriguez, M.J. Climent, S. Iborra, V. Fornes, A. Corma, J. Catal. 192 (2000) 441.
[15] S. Laforge, D. Martin, J.L. Paillaud, M. Guisnet, J. Catal. 220 (2003) 92.
[16] J. Rigoreau, S. Laforge, N.S. Gnep, M. Guisnet, J. Catal. 236 (2005) 45.
[17] T.F. Degnan Jr., J. Catal. 216 (2003) 32.
[18] J.S. Beck, A.B. Dandekar, T.F. Degnan Jr., in: M. Guisnet, J.P. Gilson (Eds.), Zeolites for Cleaner Technologies, in: Catalytic Science Series, vol. 3, Imperial College Press, London, 2002, p. 223.
[19] G.D. Pirngruber, K. Seshan, J.A. Lercher, J. Catal. 190 (2000) 396.
[20] A. Corma, C. Corell, J. Perez-Pariente, Zeolites 15 (1995) 655.
[21] G. Seo, H.S. Jeong, D.-L. Jang, D.L. Cho, S.B. Hong, Catal. Lett. 41 (1996) 189.
[22] S.L. Lawton, A.S. Fung, G.J. Kennedy, L.B. Alemany, C.D. Chang, G.H. Hatzikos, D.N. Lissy, M.K. Rubin, H.K.C. Timken, S. Steuernagel, D.E. Woessner, J. Phys. Chem. 100 (1996) 3788.
[23] M. Hunger, S. Ernst, J. Weitkamp, Zeolites 15 (1995) 188.
[24] W. Kolodziejski, C. Zicovich-Wilson, C. Corell, J. Perez-Pariente, A. Corma, J. Phys. Chem. 99 (1995) 7002.
[25] G. Engelhardt, D. Michel, High-Resolution Solid State NMR of Silicates and Zeolites, Wiley, Chichester, 1987.
[26] P. Meriaudeau, C. Naccache, Adv. Catal. 44 (1999) 505.
[27] S. van Donk, J.H. Bitter, K.P. de Jong, Appl. Catal. A 212 (2001) 97.
[28] G.D. Pirngruber, O.P.E. Zinck-Stagno, K. Seshan, J.A. Lercher, J. Catal. 190 (2000) 374.
[29] H.H. Mooiweer, K.P. de Jong, B. Kraushaar-Czarnetzki, W.H.J. Stork, B.C.H. Krutzen, Stud. Surf. Sci. Catal. 84 (1994) 2327.
[30] W.-Q. Xu, Y.-G. Yin, S.L. Suib, J.C. Edwards, C.-L. O'Young, J. Phys. Chem. 99 (1995) 9443.
[31] M. Guisnet, P. Andy, N.S. Gnep, E. Benazzi, C. Travers, J. Chem. Soc. Chem. Commun. (1995) 1685.
[32] S.-H. Lee, C.-H. Shin, S.B. Hong, J. Catal. 223 (2004) 200.
[33] B. de Menorval, P. Ayrault, N.S. Gnep, M. Guisnet, J. Catal. 230 (2005) 38.
[34] S.B. Hong, E.G. Lear, P.A. Wright, W. Zhou, P.A. Cox, C.-H. Shin, J.-H. Park, I.-S. Nam, J. Am. Chem. Soc. 126 (2004) 5817.
[35] G.D. Pirngruber, K. Seshan, J.A. Lercher, J. Catal. 186 (1999) 188.
[36] P. Biloen, F.M. Dautzenberg, W.M.H. Sachtler, J. Catal. 50 (1977) 77.
[37] M. Pan, J.M. Cowley, I.Y. Chan, Catal. Lett. 5 (1990) 1.
[38] M. Pan, Micron 27 (1996) 219.
[39] N.Y. Chen, T.F. Degnan Jr., C.M. Smith, Molecular Transport and Reaction in Zeolites, VCH, New York, 1994.
[40] H.G. Karge, Stud. Surf. Sci. Catal. 137 (2001) 707.